CHEMICAL ENGINEERING TRANSACTIONS
VOL. 70, 2018
A publication of AIDIC
The Italian Association of Chemical Engineering
Online at www.aidic.it/cet
Guest Editors: Timothy G. Walmsley, Petar S. Varbanov, Rongxin Su, Jiří J. Klemeš

ISBN 978-88-95608-67-9; **ISSN** 2283-9216
DOI: 10.3303/CET1870221

Renewable H_2 Production via Oxidative Reforming on Ni Catalysts: an Experimental and Kinetic Study

Vincenzo Palma, Concetta Ruocco*, Antonio Ricca

Departmnent of Industrial Engineering, University of Salerno, Via Giovanni Paolo II, 132, FIsciano (SA), Italy
cruocco@unisa.it

The oxidative dry reforming of a simulated biogas mixture was carried out from 400 to 800°C at ambient pressure. Catalytic tests were performed over 10 wt% Ni catalysts, prepared by wet impregnation, and Al_2O_3, CeO_2, and CeO_2-ZrO_2 were selected as catalytic supports. The results of catalysts characterization revealed the highest specific surface area of the Ni/Al_2O_3 sample and the relevant reducibility of the CeO_2-ZrO_2 based catalyst. Activity measurements proved that Ni catalysts supported on Al_2O_3 assured slightly higher CH_4 conversion and H_2 yield, compared to the CeO_2-based samples. Ni/Al_2O_3 catalyst was tested under conditions away from thermodynamic equilibrium and a kinetic model was developed and validated based on the results of experimental tests: in the investigated temperature interval, the kinetics of the reaction is satisfactory described by CH_4 total oxidation, CH_4 dry reforming and reverse water gas shift pathways.

1. Introduction

In the search for greener energy sources to replace fossil fuels, renewables based technologies (including wind, solar, geothermal and biomass power) are gaining increasing attention. Biogas is a clean fuel, mainly containing methane and carbon dioxide (50–60 % CH_4, 40 % CO_2, 1 % H_2O with traces of NH_3 in the range 80–100 ppm and H_2S in the range 30-170 ppm, depending on the feedstock) (Pirola et al., 2015) and is produced by anaerobic digestion processes of biomass or animal manure. The employment of biogas mixture as direct energy source (i.e. combustion) is discouraged, as CO_2 decreases the heating value and the flame stability of the gas mixture. In fact, with respect to pure CH_4 or natural gas, an increase of CO, NO_x and unburnt hydrocarbons is observed during combustion (Khon et al., 2011). Conversely, it can be useful to separate carbon dioxide from biogas to produce a pure methane stream via membrane separation, pressure swing adsorption or amine scrubbing. However, the costs of these processes are often prohibitive. On the other hand, reforming technology (dry, steam and/or oxidative) provides a viable route to exploit the energy contained in the biogas. In view of producing syngas, dry reforming of biogas (DRB) is regarded as the most promising alternative, which allows the simultaneous conversion of two inexpensive and greenhouse gases. Moreover, compared to steam reforming, DRB can theoretically provide a hydrogen to carbon monoxide ratio close to one, particularly appropriate for Fischer-Tropsch synthesis in the field of liquid hydrocarbon production (de Caprariis et al., 2015). However, several pathways are involved in this reaction, including reverse water gas shift (R-WGS), CO disproportion and CH_4 decomposition (de Caprariis et al., 2016): coke formation via the latter two reactions is the main cause of catalyst deactivation during dry reforming of biogas. Catalytic conversion of biogas can also be carried out using air as co-reactant: air combustion with a portion of methane can provide the heat to drive the endothermic dry reforming reaction and the additional oxidant agent may reduce carbon formation on catalyst surface. As previously observed, oxygen can adsorb on the active sites of catalyst surface and then preferentially react with carbon atoms onto the active sites (Lai et al., 2012). Therefore, depending on the selected feeding conditions, methane partial oxidation or complete combustion (OX) may occur.

In order to reach high performance and low coke selectivity during biogas reforming, proper catalytic systems are needed. Looking at the catalysts economic impact, nickel is widely selected as active species for reforming process. Despite Nickel catalysts suffer from problems related to coking and active species dispersion, it was shown that, if a strong nickel-support interaction exists, nickel sintering and carbon

Please cite this article as: Palma V., Ruocco C., Ricca A., 2018, Renewable h2 production via oxidative reforming on ni catalysts: an experimental and kinetic study , Chemical Engineering Transactions, 70, 1321-1326 DOI:10.3303/CET1870221

deposition can be avoided. Therefore, using the proper type of catalytic supports is a viable route to improve nickel catalysts activity and stability. Nickel based alumina catalysts (Ni/Al_2O_3) have been recognized as the most effective materials for methane reforming reactions, due to their low cost, good mechanical resistance, high surface area and activity (Ugarte et al, 2017). In the attempt of inhibiting coke growth on Ni-based catalysts (promoted by Lewis acidity of alumina sites), CeO_2-containing materials have been also investigated: the very quick reduction of Ce^{4+} to Ce^{3+} as well as the creation of oxygen vacancies are expected to improve catalyst reducibility and activity for biogas reforming (Turchetti et al., 2013).
In this paper, the catalytic performance of Ni-based catalysts, prepared by wet impregnation and supported on Al_2O_3, CeO_2 and CeO_2-ZrO_2, was investigated for oxidative dry reforming of biogas at T=400-800°C, CO_2/CH_4=1 and O_2/CH_4=0.6. Moreover, a kinetic investigation of DRB on the most active catalyst was carried out.

2. Experimental

2.1 Preparation and characterization of the catalysts

The 10 wt% Ni catalysts were prepared by conventional wet impregnation of $Ni(NO_3)_2{\cdot}6H_2O$ (Strem Chemicals supplier) onto commercial supports previously calcined: Al_2O_3 (Baikowski), CeO_2 (Rhodia), CeO_2-ZrO_2 (Rhodia).The impregnated solids were dried overnight at 120°C and calcined in a muffle furnace at 800°C for 3 h (with a heating rate of $10°C{\cdot}min^{-1}$).
Chemical composition was determined by X-ray fluorescence (XRF) on a ThermoFischer QUANT'X EDXRF spectrometer equipped with a rhodium standard tube as the source of radiation. The specific surface area of the supports and the final catalysts was determined by nitrogen adsorption at -196°C using the BET method with a SORPTOMETER 1040 "Kelvin" supplied Costech Analytical Tecnologies. Prior to analysis, each catalyst sample was evacuated at 150 °C for 30 min in helium flow to ensure that there was no adsorbed moisture on the catalyst surface. Temperature programmed reduction (TPR) measurements were carried out in situ before catalytic tests: reduction was performed under a 5 $\%H_2$ in N_2 stream (850 $Ncm^3{\cdot}min^{-1}$) from ambient temperature to 1100°C at a constant ramping rate of $10°C{\cdot}min^{-1}$.

2.2 Catalytic activity tests

The catalytic performance of the calcined catalysts was evaluated in a quartz tubular fixed bed reactor (i.d. 25 mm) in the laboratory apparatus described elsewhere (Palma et al. 2017). The powder was pressed, crushed and sieved to 180-355 µm particles. Typically, the reactor was charged with a constant weight of 1.9 g of the catalyst granules. After catalyst reduction in situ, a mixture of reactants feed (850 $Ncm^3{\cdot}min^{-1}$, 20% CH_4- 20 % CO_2-12 % O_2-48 % N_2) was introduced to the reactor with air being fed through an independent line (in order to avoid the contribution of homogeneous reactions). All the lines downstream the reactor was heated at 120°C to prevent water condensation. The activity tests were carried out from 400 to 800°C and products gas distribution was monitored online by means of an FT-IR spectrophotometer (supplied by ThermoScientific). Then, the effluent stream passed through a water-trap and H_2 as well as O_2 contents were determined by thermocondutivity and paramagnetic analysers, respectively (from ABB). Experimental data were compared in terms of methane conversion (X) and hydrogen yield (Y), defined as reported in Eq. 1 and 2. Kinetic studies under differential conditions were conducted in the same laboratory plant. The mass of catalyst used was 300 mg, diluted with inert quartz (500-710 µm, $V_{catalyst}$:V_{quartz} = 20:1) to avoid temperature gradients. By properly adjusting the total flowrate, methane conversion was kept below 50 %.

$$X = \frac{mol_{CH4,in} - mol_{CH4,out}}{mol_{CH4,in}} \cdot 100 \quad (1)$$

$$Y = \frac{mol_{H2,out}}{2 \cdot mol_{CH4,in}} \cdot 100 \quad (2)$$

3. Results and discussion

3.1 Physiochemical and reducibility properties of supports and final catalysts

For all the impregnated samples, the Ni wt% measured by XRF was very close to the expected value of 10, confirming that the deposition of all Ni species occurred on the support, with negligible losses (Table 1). The

results shown in Table 1 also display that the sequence of specific surface area for the catalysts was consistent with the trend of the supports. However, the specific surface areas of the catalysts were obviously decreased compared to those of the supports, which may be caused by nickel species entering into supports pores during impregnation. As can be seen, Al_2O_3 based samples exhibited the highest BET area (89 $m^2 \cdot g^{-1}$), while a value of 15 $m^2 \cdot g^{-1}$ was measured for the Ni/CeO_2 catalyst.

Table 1: Results of XRF and BET measurements.

Sample	Ni content (wt%)	SSA ($m^2 \cdot g_{cat}^{-1}$)
Al_2O_3	-	94
CeO_2	-	46
CeO_2-ZrO_2	-	61
Ni/Al_2O_3		89
Ni/CeO_2		15
Ni/CeO_2-ZrO_2		42

TPR profiles of the Ni catalysts were reported in Figure 1 in order to compare the effect of support type on the reducibility of nickel oxide. Quantitative data of hydrogen consumption were acquired from TPR curves by means of the software the software Microcal Origin. Concerning the Ni/CeO_2 catalyst, it is possible to observe three main reduction peaks centring at 213, 375 and 448°C. The low temperature peak, accounting for a H_2 consumption of 289 $\mu molH_2 \cdot g_{cat}^{-1}$, is due to the reduction of the isolated (free) NiO particles on ceria. Conversely, H_2 consumption centred above 350°C can be associated to the reduction of Ni particles strongly bonded with the support while the peak at higher temperatures was related to the partial reduction of Ce^{4+} to Ce^{3+}. The total experimental uptake (2126 $\mu molH_2 \cdot g_{cat}^{-1}$) is higher than the value estimated for the total reduction of NiO to Ni on 10 wt%Ni/CeO_2 (1704 $\mu molH_2 \cdot g_{cat}^{-1}$), which confirms that not only NiO but also CeO_2 is reduced during the measurements (Tada et al., 2017). When Ni is supported on CeO_2-ZrO_2, an increase in the contribution of high temperature reduction was observed: for example, the peak above 400°C accounted for 298 $\mu mol_{H2} \cdot g_{cat}^{-1}$ over Ni/CeO_2 while the H_2 consumption centred at 542 °C involved 1466 $\mu molH_2 \cdot g_{cat}^{-1}$ in the case of ceria-zirconia based catalysts, demonstrating that ceria is much easier reducible and oxygen species transfer much more effectively over the Ni/CeO_2-ZrO_2 catalyst (Palma et al., 2015). According to the literature, the peak observed above 500°C on the Ni/Al_2O_3 catalyst can be ascribed to the reduction of highly dispersed non-stoichiometric amorphous nickel aluminate spinel; the broad peak centred above 800°C was attributed to reduction of larger strongly interacted fraction of Ni species (diluted $NiAl_2O_4$-like phase), probably occupying the defective tetrahedral sites of alumina by bulk diffusion (López-Fonseca et al., 2017). In comparison with the TPR profiles of Ni/CeO_2 and Ni/CeO_2-ZrO_2, the reduction of the Al_2O_3-based catalyst occurred at higher temperatures and the total uptake (1535 $\mu molH2 \cdot g_{cat}^{-1}$) is slightly lower than the value required for the complete reduction of nickel oxide. Therefore, the reduction of NiO was quite difficult, which means that the interaction between Ni and Al_2O_3 is much stronger than that in the rare-earth oxides based samples (Zheng et al., 2008).

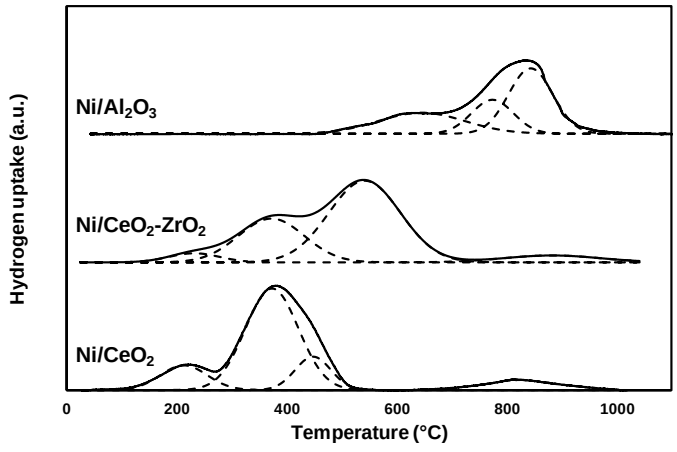

Figure 1: H_2-TPR profiles of the Ni-based catalysts

3.2 Results of biogas reforming tests and kinetic model

The results of oxidative dry reforming tests in terms of methane conversion (X) as well as hydrogen yield (Y) are shown in Figure 2, in comparison with thermodynamic predictions. Chemical equilibrium calculations were

performed by means of the software Gaseq, based on the method of free Gibbs energy minimization. According to equilibrium predictions, under oxidative dry reforming conditions, dominant reactions at low, medium and high temperatures are combustion, exothermic partial oxidation and endothermic dry reforming. Consequently, methane conversion is high in the whole temperature interval (Hadian et al., 2013). By fixing the GHSV to 10.7 $NL_{biogas} \cdot h^{-1} \cdot g_{cat}^{-1}$, the O_2 conversion is 100% starting from 400 to 800°C for all the samples. This result is in agreement with chemical equilibrium calculations: as both CO_2 and O_2 acts as co-oxidants in the combined dry-oxidative reforming process, methane reacted more easily with O_2 since CO_2 is a very stable species with led to a total O_2 conversion (Amin et al., 2007). For all the investigated catalysts, X well followed equilibrium values, especially at T > 700°C. By increasing temperature, the contribution of exothermic reactions reduces and hence the H_2 yield is mainly determined by dry reforming. Also in terms of hydrogen yield, the Ni-based catalysts displayed a fairly good agreement with thermodynamic predictions. At intermediate temperatures, the decreased hydrogen yields observed in Figure 2 can be linked to the reverse water gas shift pathway, which accounts for the increased amounts of CO_2 in the effluent streams (not shown). However, from both the diagrams of Figure 2, the slightly higher performance of Ni/Al_2O_3 catalyst were observed, which better followed equilibrium in the whole temperature interval. Moreover, for all the tested samples, water production (not shown) below 500°C is lower than the expected value (10.5 %), attesting a higher extent of reforming/shift reactions which allowed an improvement in hydrogen yield at low temperatures. Therefore, the latter sample was further tested at low contact time, in order to develop a mathematical model able to predict the kinetics of the reaction. The improved performances of the alumina-based catalyst are in agreement with the results of physiochemical characterization: despite CeO_2-containing materials display high reducibility, which is expected to improve catalyst activity, for Ni/Al_2O_3 sample a very high specific surface area, was measured. For reforming reactions, different authors (Dong et al., 2002) highlighted the key role of nickel dispersion on catalytic performances, which justify the results obtained in this study. In fact, it was reported that, in the case of finely dispersed Ni particles, the ensemble size on the metal surface becomes smaller, resulting in a higher resistance towards deactivation, as the ensemble size necessary for coke formation is larger than that for methane reforming (Rostrup-Nielsen et al., 1994).

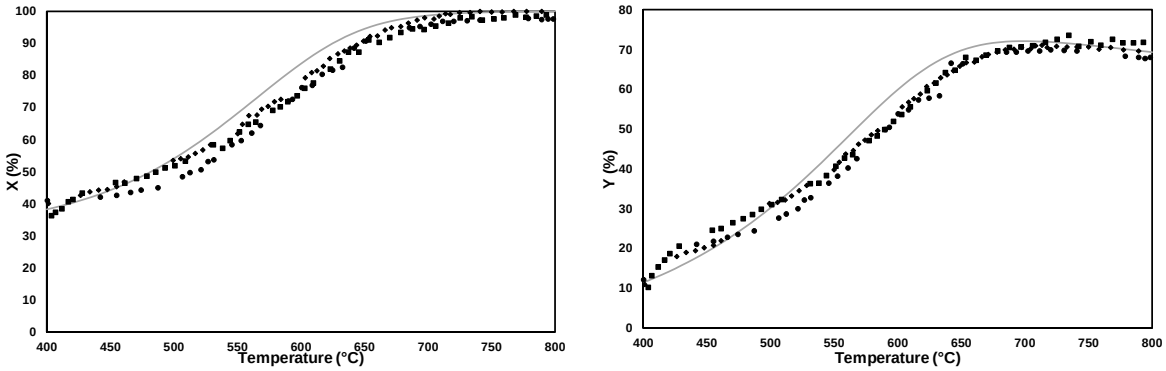

Figure 2: Equilibrium predicted (continuous line) and experimental (Ni/Al_2O_3 diamond, Ni/CeO_2 square, Ni/CeO_2-ZrO_2 circle) CH_4 conversion and H_2 yield; CH_4/CO_2=1, O_2/CO_2=0.6; GHSV=10.7 $NL_{biogas} \cdot h^{-1} \cdot g_{cat}^{-1}$.

In order to perform a simulation study of oxidative dry reforming of biogas in the fixed-bed reactor, a one-dimensional homogeneous model was applied, with concentration gradients being accounted only in axial direction. Table 2 reports the reaction rate equations and the thermodynamic constants as a function of reaction temperature (the equation is valid between 650 and 850°C) for the Eq. 3 (DRB), 4 (R-WGS) and 5 (OX).

$$CH_4 + CO_2 \leftrightarrow 2CO + 2H_2 \qquad \Delta H^{\circ}_{298K} = 247\ kJ \cdot mol^{-1} \tag{3}$$

$$CO_2 + H_2 \leftrightarrow CO + H_2O \qquad \Delta H^{\circ}_{298K} = 46.1\ kJ \cdot mol^{-1} \tag{4}$$

$$CH_4 + 2O_2 \leftrightarrow CO_2 + 2H_2O \qquad \Delta H^{\circ}_{298K} = 890.4\ kJ \cdot mol^{-1} \tag{5}$$

A simple power-law model was used to describe the rate of formation of each product (Table 2). The mathematical model was based on the hypothesis if an isothermal tubular plug flow reactor with a fixed bed of catalyst (300 mg). The model, involving the continuity equations for the various components, was implemented in the software Microsoft Excel Office 2016. To solve the differential equations, the Euler method

was used to integrate the system: the molar flow rate of every component was evaluated at every step (W+ΔW, with ΔW = 10^{-5} g). After the solution of the mass balance, the results of the model were compared with the experimental values, through an objective function which involves the minimization of the differences between the above values through the least squares method, using the kinetic constants as the variable terms. A total gas flow-rate of 850 $Ncm^3 \cdot min^{-1}$ at atmospheric pressure, with 20 % of methane, 20 % of carbon dioxide and 12 % of oxygen was fed to the reactor; the calculation was based on the experimental results recorded between 650 and 830 °C. Figure 2 compares the experimental points with the results of the power-low model. The model assures a fairly good agreement with experimental points, which indicates that the hypothesized set of reactions is possible especially at temperatures higher than 750 °C. In fact, at lower temperatures, the calculated molar flows of carbon monoxide, hydrogen and water are slightly different from experimental points, probably due to misleading R-WGS kinetic model estimation. The kinetic parameter values obtained from model regression to experimental data are summarized in Table 3. The activation energy found for total oxidation of methane is very close to previous studies (van Giezen et al., 1999), which reported a value of 151 $kJ \cdot mol^{-1}$. In addition, Ea_1 is similar to the values reported in the literature for Ni/Al_2O_3 catalysts (Nguyen et al., 2017). However, a more detailed analysis of the proposed model reveals that the reverse water gas shift reaction operates very close to thermodynamic equilibrium conditions, which was previously reported for CH_4-CO_2 reforming (Bradford et al., 1996). As a consequence, the concentration profiles for carbon monoxide and hydrogen, predicted by the model, are very close one to each other.

Table 2: Expressions for reaction rates and thermodynamic constants.

Reaction	Rate	Equilibrium constant
DRB	$r_1 = k_1\left(P_{CH4}P_{CO2} - \frac{P_{CO}^2 P_{H2}^2}{Keq_1}\right)$	$K_{eq1} = 2.1 \cdot 10^{15} \cdot T^{-1.21} \cdot \exp\left(-\frac{5389}{T}\right)$ $Keq_1\ [=] atm^2$
R-WGS	$r_2 = k_2\left(P_{CO2}P_{H2} - \frac{P_{CO}P_{H2O}}{Keq_2}\right)$	$K_{eq2} = 6.3 \cdot 10^{5} \cdot T^{-0.14} \cdot \exp\left(-\frac{31448}{T}\right)$ $Keq_2\ [=] -$
OX	$r_3 = k_3 P_{CH4} P_{O2}^2$	-

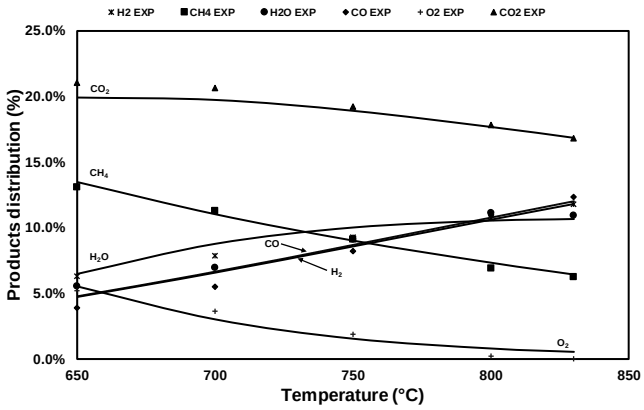

Figure 2: Experimental (points) and model (lines) products distribution as a function of reaction temperature; CH_4/CO_2=1, O_2/CO_2=0.6; GHSV=68 $NL_{biogas} \cdot h^{-1} \cdot g_{cat}^{-1}$.

Table 3: Pre-exponential factors (ko) and activation energy (Ea) of the power-low model.

Parameter	Value	Units
$\boldsymbol{k0_1}$	$5.8 \cdot 10^3$	$mol \cdot h^{-1} \cdot g_{cat}^{-1} \cdot atm^{-2}$
$\boldsymbol{Ea_1}$	66	$kJ \cdot mol^{-1}$
$\boldsymbol{k0_2}$	$9.7 \cdot 10^9$	$mol \cdot h^{-1} \cdot g_{cat}^{-1} \cdot atm^{-2}$
$\boldsymbol{Ea_2}$	154	$kJ \cdot mol^{-1}$
$\boldsymbol{k0_3}$	$9.8 \cdot 10^{-1}$	$mol \cdot h^{-1} \cdot g_{cat}^{-1} \cdot atm^{-2}$
$\boldsymbol{Ea_3}$	11	$kJ \cdot mol^{-1}$

4. Conclusions

Ni-based samples were prepared by wet impregnation as catalysts for oxidative dry reforming of biogas between 400 and 800°C under a 20 %CH_4 / 20 %CO_2 / 12 %O_2 stream. A relevant reducibility was recorded over the rare earth oxides-based materials. At a space velocity of 10.7 $NL_{biogas} \cdot h^{-1} \cdot g_{cat}^{-1}$, a fairly good agreement with thermodynamic predictions was observed for all the catalysts. However, the Ni/Al_2O_3 sample displayed the highest specific surface area, which also resulted in improved performance for the above reaction. A mathematical model to predict product gas distribution over the Ni/Al_2O_3 catalyst was also developed, accounting for dry reforming of biogas, methane total oxidation, and reverse water gas shift reaction. The model well fitted experimental data above 750°C and reverse water gas shift pathway was found very close to thermodynamic equilibrium predictions.

References

Amin N.A.S., Yaw T.C., 2007, Thermodynamic equilibrium analysis of combined carbon dioxide reforming with partial oxidation of methane to syngas, International Journal of Hydrogen Energy, 32, 1789-1798.

Bradford M.C., M.A. Vannice, 1996, Catalytic reforming of methane with carbon dioxide over nickel catalysts II. Reaction kinetics, Applied Catalysis A: General, 142, 97-122.

de Caprariis B., De Filippis P., Petrullo A., Scarsella M., 2015, Methane dry reforming over nickel perovsikite catalysts, Chemical Engineering Transactions, 43, 991-996.

de Caprariis B., de Filippis P., Palma V., Petrullo A., Ricca A., Ruocco C., Scarsella M., 2016, Rh, Ru and Pt ternary perovskites type oxides $BaZr_{(1-x)}Me_xO_3$ for methane dry reforming, Applied Catalysis A: General, 517, 47-55.

Dong W.-S., Roh H.-S., Jun K.-W., Park S.-E., Oh Y.-S., 2002, Methane reforming over Ni/Ce-ZrO_2 catalysts: effect of nickel content, Applied Catalysis A: General, 226, 63-72.

Hadian N., Rezaei M., 2013, Combination of dry reforming and partial oxidation of methane over Ni catalysts supported on nanocrystalline $MgAl_2O_4$, Fuel, 113, 571-579.

Kohn M.P., Lee J., Basinger M.L., Castaldi M.J., 2011, Performance of an internal combustion engine operating on landfill gas and the effect of syngas addition, Industrial & Engineering Chemistry Research, 50, 3570-3579.

Lai M.-P., Lai W.H., Horng R.F., Chen C.Y., Chiu W.C., Su S.S., Chang Y.M., 2012, Experimental study on the performance of oxidative dry reforming from simulated biogas, Energy Procedia, 29, 225-233.

López-Fonseca R., Jiménez-González C., Gil-Calvo M., de Rivas B., Gutiérrez-Ortiz J.-I., 2017, Partial oxidation of gasoline over ni/al_2o_3 catalysts using nickel aluminate as precursor, Chemical Engineering Transactions, 57, 955-960.

Nguyen T., Łamacz A., Krztoń A., Ura A., Chałupka K., Nowosielska M., Rynkowski J., Djéga-Mariadassou G., 2015, Partial oxidation of methane over Ni^0/La_2O_3 bifunctional catalyst II: Global kinetics of methane total oxidation, dry reforming and partial oxidation, Applied Catalysis B: Environmental, 165, 389-398.

Palma V., Ruocco C., Ricca A., 2015, Bimetallic Pt and Ni Based Foam Catalysts for Low-Temperature Ethanol Steam Reforming Intensification, Chemical Engineering Transactions, 43, 559-564.

Palma V., Ruocco C., Ricca A., Meloni M., 2017, Coke-resistant Pt-Ni/CeO_2-SiO_2 catalysts for ethanol reforming, Chemical Engineering Transactions, 57, 1675-1680.

Pirola C., Galli F., Mamenti F., Bianchi C., 2015, Biogas upgrading by physical water washing in a micro-pilot absorption column at low temperature and pressure, Chemical Engineering Transactions, 43, 1207-1211.

Rostrup-Nielsen J.R., 1994, Aspects of CO_2-reforming of Methane, Studies in Surface Science and Catalysis, 81, 25-41.

Tada S., Shimizu T., Kameyama H., Haneda T., Kikuchi R., 2017, Ni/CeO_2 catalysts with high CO_2 methanation activity and high CH_4 selectivity at low temperatures, International Journal of Hydrogen Energy, 37, 5527-5531.

Turchetti L., Monteleone G., Giaconia A., Sau S., Palma V., Castaldo F., Lemonidou A, Angeli S., 2013, Time-on-Stream stability of new catalysts for low-temperature steam reforming of biogas, Chemical Engineering Transactions, 35, 685-690.

Ugarte P., Durán P., Lasobras J., Soler J.,Menéndez M., Herguido J., 2017, Dry reforming of biogas in fluidized bed: Process intensification, International Journal of Hydrogen Energy, 42, 13589-13597.

van Giezen J.C., van den Berg F.R., Kleinen J.L., van Dillen A.J., Geus J.W., 1999, The effect of water on the activity of supported palladium catalysts in the catalytic combustion of methane, Catalysis Today, 47, 287-293.

Zheng W., Zhang J., Ge Q., Xu H., Li W., 2008, Effects of CeO_2 addition on Ni/Al_2O_3 catalysts for the reaction of ammonia decomposition to hydrogen, Applied Catalysis B: Environmental, 80, 98-105.